VII International Conference on Computational Methods in Marine Engineering
MARINE 2017
M. Visonneau, P. Queutey and D. Le Touzé (Eds)

EXTENSION OF THE TURBULENT SPOT METHOD TOWARDS ARBITRARY REYNOLDS STRESSES AND INTEGRAL LENGTHS

HANNES KRÖGER*, NIKOLAI KORNEV† AND PASCAL ANSCHAU**

*Chair of Modeling and Simulation (LEMOS)
University of Rostock, Albert-Einstein-Str. 2, 18059 Rostock, Germany
e-mail: hannes.kroeger@uni-rostock.de, web page: http://www.lemos.uni-rostock.de/

†Chair of Modeling and Simulation (LEMOS)
e-mail: nikolai.kornev@uni-rostock.de

**Schiffbau-Versuchsanstalt Potsdam GmbH
Marquardter Chaussee 100, 14469 Potsdam, Germany
e-mail: anschau@sva-potsdam.de, web page: http://www.sva-potsdam.de/

Key words: Large-Eddy simulation, inflow boundary condition, turbulence synthesis

Abstract. The paper presents an extension of the Turbulent Spot method which enables to obey the continuity of the fluctuations while producing arbitrarily high anisotropy at the same time. The derivation of the structures is summarized and expressions for their Reynolds stresses and length scales are presented. Finally, the newly derived structures are applied to a turbulent channel flow simulation and compared with other means of turbulence synthesis.

1 INTRODUCTION

In many engineering problems, accuracy of the Reynolds averaged Navier Stokes (RANS) simulations is not sufficient and a more detailed information on the properties of turbulence are required than these which RANS solution provides. A possible remedy is to employ scale resolving techniques like Direct Numerical Simulation (DNS) or Large Eddy Simulation (LES). While DNS still remains out of reach, LES has become a viable option even for industrial users due to constantly increasing power of modern computers. In this context, an important development during the last decades are hybrid RANS/LES methods which extend the applicability of scale resolving methods far towards high Reynolds number flows by excluding the expensive near-wall region from LES and applying unsteady RANS there.

The domain in a flow simulation is always bounded by in- and outlets. Proper boundary conditions at these boundaries have to be prescribed in a CFD simulation of the flow device,

especially at the inlet. In common engineering practice, the flow through the inlet is already turbulent. In RANS context, mean quantities and integral properties of the turbulent fluctuations then have to be prescribed. In contrast, scale resolving simulation techniques gain their advantage by directly including the turbulent fluctuation velocities in the solved velocity field. Thus, the turbulent content at inlet boundaries has to be explicitly prescribed in terms of an unsteady velocity field.

Formulation of the inlet condition is a well-recognized topic in LES and DNS research. Overview of existing methods can be found e.g. in [18, 15, 6, 5, 16, 12]. According to Schlüter et al. [15] the methods for specification of turbulent inlet conditions utilize one of four following techniques:

1. natural laminar turbulent transition,
2. random uncorrelated oscillations,
3. LES or DNS auxiliary simulation with periodic boundary conditions in a domain in front of the area of interest,
4. synthetic turbulent fields.

First two techniques are nowadays not used because the first one requires huge computational resources whereas the second one generates uncorrelated fields which quickly dissipate behind the inlet.

The third approach is widely used for flows with any dominating flow direction. In many cases, when the flow domain is a continuation of pipe or channel flows, the use of periodic boundary conditions in auxiliary domain is the most efficient way to generate inlet conditions. For flows with change of averaged parameters in auxiliary simulation domain, such as, for instance, boundary layers, Spalart proposed the recycling method [17]. In this case the modified periodic boundary conditions are enforced in which the data from outlet to inlet are copied with some rescaling factor. Extension of this technique to three dimensional flows is quite difficult because the recycling direction is hard to detect. A proper development of perturbations in auxiliary domain requires a certain length. To reduce this length, a special forcing within the auxiliary domain is introduced in [1] and [13]. The forcing term is added as an additional body force to control the integral parameters of the boundary layer evolving in the auxiliary domain. The biggest weakness of the third approach is the complexity of its application for arbitrary geometries.

Within the last approach the turbulence is artificially generated without solution of flow equations. The task is to synthesize a turbulent velocity field $\mathbf{U}(\mathbf{x}, t)$:

$$\mathbf{U}(\mathbf{x}, t) = \overline{\mathbf{U}}(\mathbf{x}) + \mathbf{u}(\mathbf{x}, t) \tag{1}$$

where $\overline{\mathbf{U}}(\mathbf{x})$ is the mean velocity which is supposed to be known. The fluctuations $\mathbf{u}$ need to have a number of properties, which we, according to our experience, list below in the order of their importance:

1. $\mathbf{u}$ should be spatially and temporally correlated.
2. They have to possess prescribed Reynolds stresses $R_{ij} = \overline{u_i u_j}(\mathbf{x})$.

3. Additionally to the requirement 1, $\mathbf{u}$ has to possess prescribed integral lengths $L_{ij}(\mathbf{x}, \mathbf{e}_\eta) = \int_0^\infty \rho_{ij}(\mathbf{x}, \eta\mathbf{e}_\eta)d\eta$.
4. $\mathbf{u}$ should fulfill the continuity constraint $\nabla \cdot \mathbf{u} = 0$.
5. Additionally to the requirements 1 and 3, $\mathbf{u}$ should have prescribed correlation functions $r_{ij}(\mathbf{x}, \boldsymbol{\eta}) = \frac{\overline{u_i(\mathbf{x},t)u_j(\mathbf{x}+\boldsymbol{\eta},t)}}{\overline{u_i(\mathbf{x},t)u_j(\mathbf{x},t)}}$ or prescribed spectra.

Artificial turbulence always needs a certain distance (adaption distance) to evolve into real turbulence. Violation of these requirements can lead to an extension of adaption distance.

The requirement 4 is especially important for applications where a volumetric oscillation field is necessary. For the plane inlet, the derivative perpendicular to the inlet can make sense by utilization of the Taylor hypothesis. It is assumed that the inlet is far from the area of strong flow change and the turbulence can be considered as a frozen one close to the inlet. Our experience shows that the violation of req. 4 can lead to a weak convergence of the iterative process for solution of the flow equations or artificial pressure fluctuations (i.e. noise) in the flow domain. Usually, in existing methods only the requirements 1 and 2 are satisfied. To fulfill the req. 5, either the correlation function or spectrum should be specified which are usually not available for complex flows. The condition 3 thus represents a relaxed constraint where not the shape of correlation function needs to be known but only its integral.

The current work deals with a method for turbulence synthesis with the special focus on fulfillment of the continuity constraint by retaining arbitrary anisotropy in the Reynolds stresses. We propose the extension of the turbulent spot method based on exact mathematical solutions which fulfills the requirements 1-4. In the next section we briefly outline the mathematical basis of the method.

2 TURBULENT SPOT METHOD

2.1 Non-solenoidal version of the method

The initial version of the method has been developed and published in 2003 for inhomogeneous non-solenoidal turbulent fields [7]. The starting point for the development of the turbulent spots (TS) method were works in which turbulence was simulated by a set of stochastically distributed vortex structures.

The turbulent field in TS method was represented as a set of N compact spots with an inner primary velocity distribution with components $v_n^i(\mathbf{r} - \mathbf{r}^i) = \varepsilon_n^i f_n(\mathbf{r} - \mathbf{r}^i)$, where n is the component number, $\mathbf{r}^i$ is the spot center, ε_n^i is a random number, uniformly distributed between -1 and 1, and $i = 1, N$. The velocity fluctuation at any point $\mathbf{r}$ is equal to the sum of contributions of all spots $\mathbf{v} = \sum_{i=1}^{N} \mathbf{v}^i(\mathbf{r} - \mathbf{r}^i)$. The stochastic behavior of the velocity field is provided by stochastic distribution of the spots centers in space and random choice of the vector $\boldsymbol{\varepsilon}^i$. If the velocity field $\mathbf{v}$ moves through any inlet surface, which is not necessary plain, with the unit velocity $W_1 = 1$ in, say, x_1 direction, the x_1 coordinate becomes equal to time, $x_1 = Wt$. This is an application of the Taylor hypothesis often used in the turbulence research. If the signs of components of the vector $\boldsymbol{\varepsilon}^i$ are chosen statistically independently, then all one-point correlations, calculated at any fixed observation point at the inlet, satisfy the condition

$\overline{v_n v_k} = \delta_{nk} \sum_{i=1}^{N} \overline{v_n^i v_k^i}$, where overline stands for the time averaging. If a spot has a compact non zero support, the field $\mathbf{v}$ is spatially (and temporally) correlated since two point correlations $\overline{v_n(\mathbf{r}) v_k(\mathbf{r}+\boldsymbol{\eta})} = \delta_{nk} \sum_{i=1}^{N} \overline{v_n^i(\mathbf{r}) v_k^i(\mathbf{r}+\boldsymbol{\eta})}$ are not zero. Therefore, it is possible to generate the field with specified spectra (or autocorrelation function) and integral length. In this form the TS method is theoretically identical to the Synthetic Eddy Method which appeared later in [3].

2.2 Consideration of anisotropy in synthetic turbulence generators.

Since the most of turbulent flows are strongly anisotropic, the synthetically generated signal should possess the prescribed Reynolds stresses. An elegant way to consider the anisotropy was proposed in [10]. Once three components $v_i, i = 1,3$ of primary velocity are generated separately and conditioned $\overline{v_{(i)} v_{(i)}} = 1$, the secondary velocity field is calculated from the linear combination

$$u_i = a_{ij} v_j \tag{2}$$

where a_{ij} is the matrix which can be found from the condition $R_{ij} = \overline{u_i u_j} = \overline{v_m v_k} a_{im} a_{jk}$. If $\overline{v_{(i)} v_{(i)}} = 1$ and $\overline{v_i v_{j \neq i}} = 0$ the matrix satisfying $R = aa^T$ can be found from the Cholesky algorithm

$$a_{ij} = \begin{pmatrix} \sqrt{R_{11}} & 0 & 0 \\ R_{21}/a_{11} & \sqrt{R_{11} - a_{21}^2} & 0 \\ R_{31}/a_{11} & (R_{32} - a_{21} a_{31})/a_{22} & \sqrt{R_{33} - a_{31}^2 - a_{32}^2} \end{pmatrix} \tag{3}$$

Two aspects should be noted when applying this transformation: First, the cross-correlations of the primary velocities has to be zero: $\rho_{ij} = \overline{u_i u_{j \neq i}} = 0$. This is e.g. not fulfilled for the DSRFG turbulence generators while it is fulfilled for TSM and SEM. Second, the transformation affects the length scales and the spectrum of the produced fluctuations. The authors derived a modified transformation which preserves the autocorrelation functions [8].

2.3 Incorporation of divergence free condition.

A non-solenoidal character of the generated fluctuations $\nabla \vec{u} \neq 0$ was a big drawback to the turbulent spot method. Later on, the method was extended to obey the continuity condition $\nabla \mathbf{u} = 0$ by deriving the inner velocity distribution from a vector potential $\mathbf{A}$ [9]. The idea is based on the fact that the velocity field obtained as $\mathbf{u} = \nabla \times \mathbf{A}$ satisfies the continuity condition $\nabla \mathbf{u} = \nabla(\nabla \times \mathbf{A}) = 0$ automatically.

Essentially the same idea was proposed later by Poletto et al [14] who used the Biot-Savart kernel which is obtained from the condition $\mathbf{u} = \nabla \times \mathbf{A}$ with the vector potential $\mathbf{A}$ taken as the fundamental solution of the Poisson equation $\Delta \mathbf{A} = -\nabla \times \mathbf{u}$. We called this new spots of vector potential with corresponding divergence-free velocity fields as "vortons" following the term introduced by Saffman.

Unfortunately, the vortons, introduced above, are ideal for isotropic turbulence and difficult to apply for anisotropic flows close to the wall where the Reynolds stress R_{11} is much larger than the other ones. Generally, the anisotropy can be introduced in two ways. The first one is based on Cholesky transformation when three velocity components of velocity induced by

vorton are rescaled. This way is not acceptable since it results in the loss of the divergence-free property. The second way is to dismiss the Cholesky transformation and to derive anisotropic turbulent spots. In this paper we present analytical solutions for such a spot obtained for the homogeneous turbulence.

2.4 Extension towards arbitrary anisotropy with retention of the continuity condition. Derivation of anisotropic vortons

The current work utilizes another approach for introducing the anisotropy into the turbulent spots which obeys continuity and allows to reproduce strong levels of anisotropy at the same time. The approach is basically a continuation of the vorton formulation described in [9]. The generation is performed in the coordinate system (x, y, z) determined by principle axes of the Reynolds stresses. The Reynolds stresses in any other system (x', y', z') are calculated as $R'_{ij} = E_{pi}R_{pq}E_{qj}$, where E_{ij} is the rotation matrix describing coordinate transformation between (x, y, z) and (x', y', z') axes system. Integral lengths in different systems can be found from the relation:

$$L_i^i(x', y', z') = \sum_{k=1}^{3} E_{ki}^2 \frac{R_{kk}(x, y, z)}{R'_{ii}(x', y', z')} L_k^k(x, y, z) \tag{4}$$

In [9], the vector potential is scaled by a function with spherical symmetry which in case of the spectrum of decaying turbulence gives an analytic expression:

$$\mathbf{A}(x, y, z) = Ce^{-\frac{1}{2}k_0^2 r^2}\boldsymbol{\gamma} \tag{5}$$

Note that also other spectra $E(k)$ could be used in principle. This would result in different shapes of the inner velocity distribution. For the sake of simplicity and because it yields reasonably simple formulas, the current work has been restricted to this spectrum.

The spherical symmetry of $\mathbf{A}(x, y, z)$ is the reason for the isotropy of turbulence generated using these vortons. At this level, anisotropy can be introduced by stretching the coordinates individually in a similar manner as it was done in [14], i.e.

$$x \to x/\sigma_x \quad y \to y/\sigma_y \quad z \to z/\sigma_z.$$

With this, the vector potential and velocity induced by vorton are now written as:

$$\mathbf{A} = \exp\left[-\frac{1}{2}\left(\frac{x^2}{\sigma_x^2} + \frac{y^2}{\sigma_y^2} + \frac{z^2}{\sigma_z^2}\right)\right] \begin{pmatrix} x\gamma_x \\ y\gamma_y \\ z\gamma_z \end{pmatrix} \tag{6}$$

$$\mathbf{u} = \exp\left[-\frac{1}{2}\left(\frac{x^2}{\sigma_x^2} + \frac{y^2}{\sigma_y^2} + \frac{z^2}{\sigma_z^2}\right)\right] \begin{pmatrix} \left(\frac{\gamma_y}{\sigma_z^2} - \frac{\gamma_z}{\sigma_y^2}\right) yz \\ \left(\frac{\gamma_z}{\sigma_x^2} - \frac{\gamma_x}{\sigma_z^2}\right) xz \\ \left(\frac{\gamma_x}{\sigma_y^2} - \frac{\gamma_y}{\sigma_x^2}\right) xy \end{pmatrix} \tag{7}$$

Note that the multiplication with the coordinates is introduced to make the resulting Reynolds stress tensor a diagonal tensor which is identified with the diagonal matrix of eigenvalues from

a principal component analysis of the prescribed Reynolds stress tensor. By aligning the x, y, z-directions of the vorton with the principal directions of the Reynolds stress tensor, arbitrary anisotropic Reynolds stresses can be reproduced. The vorton sizes σ_x, σ_y and σ_z and strength vector components γ_x, γ_y and γ_z are free parameters of the vorton and can be used to match the prescribed Reynolds stresses and integral length scales.

2.5 Statistical properties of anisotropic vortons

Statistical properties can analytically be derived for homogeneous turbulence. We consider the set of fully uncorrelated vortons, i.e. $\overline{\gamma_{ik}\gamma_{jm}} = 0$ for each pairs of $k-th$ and $m-th$ vortons with strength components i and j. Then the Reynolds stress R_{ij} of the total field is equal to the sum of Reynolds stresses produced by each vorton

$$R_{ij} = \overline{u_i u_j} = \sum_{k=1}^{n_s} \overline{u_{ik} u_{jk}} = \sum_{k=1}^{n_s} R_{ij,k}$$

Without loss of generality we set the magnitude of the strength to be unit, i.e. $|\pm\boldsymbol{\gamma}| = 1$. Then the expectation of the Reynolds stress R_{ij} at the point $(0,0,0)$ is

$$R_{ij} = \int\limits_V u_i(\boldsymbol{\gamma}, \mathbf{x}) u_j(\boldsymbol{\gamma}, \mathbf{x}) P(\mathbf{x}) dV$$

where $P(\mathbf{x})$ is the probability density function of the event that the vorton is placed at the point $\mathbf{x}$. For the uniform distribution $P(\mathbf{x}) = n_s/V = c$ is the vorton density. If the computational domain becomes infinite n_s should increase, so that the vorton density remains constant:

$$R_{ij} = c \int\limits_{-\infty}^{\infty} \int\limits_{-\infty}^{\infty} \int\limits_{-\infty}^{\infty} u_i u_j dx dy dz \tag{8}$$

Substitution of velocity, induced by anisotropic vorton (7), in (8) results in a simple formula

$$\mathbf{R} = c\frac{\pi^{3/2}}{4} \begin{pmatrix} \frac{\sigma_x(\gamma_y\sigma_y^2 - \gamma_z\sigma_z^2)^2}{\sigma_y\sigma_z} & 0 & 0 \\ 0 & \frac{\sigma_y(\gamma_x\sigma_x^2 - \gamma_z\sigma_z^2)^2}{\sigma_x\sigma_z} & 0 \\ 0 & 0 & \frac{\sigma_z(\gamma_x\sigma_x^2 - \gamma_y\sigma_y^2)^2}{\sigma_x\sigma_y} \end{pmatrix} \tag{9}$$

2.6 Determination of anisotropic vorton parameters σ and γ.

Integration of autocorrelation functions reveals a simple and clear interpretation of stretching parameters σ_i:

$$L_x^x = \int_0^\infty \rho_{xx}(\eta_x, 0, 0) d\eta_x = \sqrt{\pi}\sigma_x$$

$$L_y^y = \int_0^\infty r_{yy}(0, \eta_y, 0) d\eta_y = \sqrt{\pi}\sigma_y$$

$$L_z^z = \int_0^\infty r_{zz}(0, 0, \eta_z) d\eta_z = \sqrt{\pi}\sigma_z$$

Therefore, the parameters σ_i are uniquely determined from the last formulas $\sigma_i = L_i^i/\sqrt{\pi}$. The vorton strength vector $\boldsymbol{\gamma}$ is found from the condition for Reynolds stresses:

$$\begin{aligned}
\gamma_y\sigma_y^2 - \gamma_z\sigma_z^2 &= \pm 2\sqrt{c^{-1}R_{11}}\frac{L_yL_z}{L_x} \\
\gamma_x\sigma_x^2 - \gamma_z\sigma_z^2 &= \pm 2\sqrt{c^{-1}R_{22}}\frac{L_xL_z}{L_y} \\
\gamma_x\sigma_x^2 - \gamma_y\sigma_y^2 &= \pm 2\sqrt{c^{-1}R_{33}}\frac{L_xL_y}{L_z}
\end{aligned} \tag{10}$$

where the upper index in L is omitted for the sake of brevity. Since the determinant of (10) is zero, a solution of the system (10) is only possible if the following condition is satisfied:

$$\pm\sqrt{R_{11}\frac{L_yL_z}{L_x}} \pm \sqrt{R_{33}\frac{L_xL_y}{L_z}} = \pm\sqrt{R_{22}\frac{L_xL_z}{L_y}}$$

or

$$L_y = \frac{\pm L_xL_z\sqrt{R_{22}}}{\pm L_z\sqrt{R_{11}} + \pm L_x\sqrt{R_{33}}}$$

The signs before different terms are independent of each other. Therefore, the integral lengths can not be arbitrary. If two length scales L_x and L_y are prescribed the remaining length should satisfy the conditions above. Particularly, this solution is wrong for the isotropic turbulence since, if $R_{22} = R_{33} = R_{11}$ and $L_x = L_z = L$, the third length is $L_y = L/2$ although all integral lengths based on longitudinal autocorrelation functions should be equal.

This limitation can be overcome by mix of two statistically independent velocity fields $\mathbf{u}_1$ and $\mathbf{u}_2$ generated using the algorithm described above. While the derivation is straightforward, this has not yet been utilized in the course of the current work.

2.6.1 Difference with SEM [14].

At this stage, the following differences with the SEM [14] can be pointed out:

- The present method is based on simple analytic function (7) which has smooth derivatives of arbitrary order. As a result the divergence free condition is satisfied everywhere within the computational domain.
- The most serious advantage is that, three integral lengths L_i can be explicitly prescribed. For that, the exact analytic relations were derived to express the vorton sizes σ_i through L_i.

2.7 Application to inhomogeneous case

The anisotropic vortons derived above and described by simple formula (7) were obtained for the homogeneous turbulence, i.e. all statistical moments are invariant with respect to translation of the reference system. Only three integral lengths scales can be specified. The autocorrelation functions cannot be specified since they are predetermined and correspond to the spectrum of

decaying turbulence. The most serious limitation of this solution is the negligence of inhomogeneity. This is due to the fact, that derivation of relations for inhomogeneous case leads to complicated nonlinear integral equations whose analytic solution is not possible. Their numerical solution is also a very laborious procedure. Instead of that we propose to use homogeneous solutions which locally neglect their interaction. With other words, at each point x, y, z we place vortons with $\sigma_i(x, y, z)$ and $\gamma_i(x, y, z)$ calculated using stresses and lengths specified at this point. Due to overlapping of vortons with different properties, resulting stresses and lengths have some deviation from the specified ones. This deviation depends on the rate of the spatial change of Re and L and sizes of vortons σ_i. For instance, in boundary layers Re stresses have the strongest gradient in normal direction y. However, as shown in the next section, it is possible to obtain satisfactory results since the overlapping is governed by σ_y which is very small near the wall.

3 IMPLEMENTATION

The Turbulent Spot method has been implemented into the open source fluid dynamics package OpenFOAM® [19, 4]. The software OpenFOAM® was chosen because of its open and modular architecture and because it is sufficiently sophisticated to apply it to almost all technically relevant flow problems.

During layout of the implementation, focus was put on easy and simple application. The Turbulent Spot method was thus implemented as a self-contained boundary condition class. As an input, only Reynolds stress and length scale distributions have to be prescribed. The population of turbulent structures is generated and maintained online during the simulation.

3.1 Algorithm

Vortons are treated in a lagrangian manner. They are continuously generated upstream of the inlet boundary and are then convected through the boundary surface. During this period, the induced velocities on the boundary faces are computed. When a vorton has passed through the inflow boundary move so far downstream, that its induced velocity on the inlet vanishes, it is deleted from the vorton population. To best fit into the unstructured grid framework of OpenFOAM®, the algorithm works on a per-face basis.

The first goal is to ensure a uniform coverage of the inlet surface with vortons. A volumetric concentration' of vortons is described by the parameter c:

$$c = \frac{n_s V_v}{V} = \frac{n_s}{V} L_1 L_2 L_3 \tag{11}$$

with the number of vortons n_s covering a space volume V and the virtual volume of a vorton expressed by the product of its integral length scales $V_v = L_1 L_2 L_3$.

The value c is an external parameter for the generation procedure. It does not influence the generated statistics directly, i.e. after a sufficiently long averaging time the generated Reynolds stresses and length scales are equal, independent from the value of c. A value much lower than unity $c \ll 1$ leads to intermittency. Large values lead to a growing number of vortons present per timestep and thus to an increase in computational effort and memory requirement. For the subsequent simulations, usually values of $c = 2$ have been used. This avoids intermittency by ensuring some reasonable amount of overlapping between neighboring vortons.

The uniform distribution of vortons in space is achieved by placing them in the swept volume of the face under consideration. Therefore, vortons are queued up with random face-normal distances, one vorton at each distance level. Each vorton is also randomly shifted within the plane parallel to its associated face, but only within the bounds of the face.

Each point in the swept volume shall have an equal probability for being chosen, which is related to the concentration parameter c

$$P(\vec{x}) = \frac{c}{V_v} \tag{12}$$

The expected distance between subsequent vortons can be derived as

$$\langle \Delta_v \rangle = \frac{V_v}{cA_f} = \frac{L_1 L_2 L_3}{cA_f} \tag{13}$$

with A_f being the area of the face under consideration. The vorton queue upstream of each face is continuously replenished so that all vortons which will affect faces during the current timestep are contained.

4 RESULTS

4.1 Channel Flow

The described method is applied to a generic channel flow test case. Channel flows essentially comprise two turbulent boundary layers at the top and bottom wall. The turbulence is anisotropic in the whole domain and isotropy is only approximately recovered in a small region near the channel mid plane. Compared to more complex flow cases, where the turbulence evolution downstream of the inlet might be quickly dominated e.g. by complicated geometry or other forcing, the turbulence in the channel is only caused by the presence of the flat wall and develops just very slowly naturally. These circumstances make the channel flow a quite challenging test case for turbulent inflow generation.

Channels with three Reynolds numbers have been simulated for which DNS results are available [11]. Parameters of all simulations are summarized in table 1.

4.1.1 Simulations with Cyclic Boundary Conditions

Conventionally, channel flow simulations are carried out without inflow turbulence generation using cyclic boundary conditions in all directions including the bulk flow direction and a mean pressure gradient for adjusting the bulk flow velocity. Such simulations have been done in advance of the inflow generator simulations to prove the mesh and numerical settings.

The results of the cyclic channel simulations suggest that the resolution and numerical settings are sufficient. The friction coefficients for all Reynolds numbers are plotted in figure 2 and the Reynolds stresses are shown in figure 1. All profiles are considered to be reasonably close to the reference values.

4.1.2 Inflow Generator Simulations

Once the numerical settings are validated, the cyclic boundaries in axial direction have been replaced by a velocity inlet/pressure outlet pair. In addition, the length of the channel was

Reynolds number Re_τ	δ $(H/2)$		Domain size $L \times H \times W$	Resolution $\Delta_x^+ \times \Delta_{y,wall}^+ \times \Delta_z^+$	Grid size $n_x \times n_y \times n_z$
180	1	cyclic BCs	$6 \times 2 \times 4.2$	$20 \times 2 \times 10$	$54 \times 48 \times 75$
		inflow BC	$12 \times 2 \times 4.2$	$20 \times 2 \times 10$	$108 \times 48 \times 75$
395	1	cyclic BCs	$6 \times 2 \times 4.2$	$20 \times 2 \times 10$	$118 \times 64 \times 165$
		inflow BC	$12 \times 2 \times 4.2$	$20 \times 2 \times 10$	$237 \times 64 \times 165$
590	1	cyclic BCs	$6 \times 2 \times 4.2$	$20 \times 2 \times 10$	$177 \times 75 \times 247$
		inflow BC	$12 \times 2 \times 4.2$	$20 \times 2 \times 10$	$354 \times 75 \times 247$

Table 1: Parameters of the channel flow simulations

increased and the pressure gradient forcing removed, because it becomes unnecessary. The parameters of these simulations are contained in table 1 as well.

Reynolds number Re_τ	turbulent structure type
180	anisotropic vorton
395	hat spot
	isotropic vorton
	anisotropic vorton
	anisotropic vorton, $R_{uv} = 0$
	DSRFG turbulence ("Modal") [2]
590	anisotropic vorton

Table 2: Inflow channel simulations: computed variants

The reynolds number Re_τ has been varied for simulations with the anisotropic vorton and for the middle Reynolds number $Re_\tau = 395$ only, the influence of the turbulent structure was evaluated.

The friction coefficient $c_f = \tau_w / \frac{1}{2}\rho u_m^2$ can be regarded as a measure of the reality level of the generated turbulence. As visible in figure 2, the friction coefficient vs. axial length should ideally be a horizontal curve. Figure 3a shows the friction coefficient evolution along the channel at $Re_\tau = 395$ for different turbulent structure types. Again, there is an initial deviation from expected value. It decreases with running length and is identified as the adaption distance. This distance depends on the type of structure used. The most primitive hat spot type needs the longest time to morph into real turbulence. A better behavior is obtained with the vorton types. With these structures, the adaption distance is about one channel height H shorter. The anisotropic vorton simulations have been carried out in two variants: with the full Reynolds stress tensor and with a diagonal-only tensor ($R_{uv} = 0$).

In the former case, since the generated primary fluctuation field is always diagonal, the off-diagonals are produced by aligning the vortons with the principal axes of the prescribed Reynolds stress tensor. Since the longitudinal length scale is large compared to the lateral ones, an oblique orientation of the vortons leads to increased smoothing of the reproduced Reynolds stress profile (compare section 2.7). Also, oblique structures intersect with the wall and thus

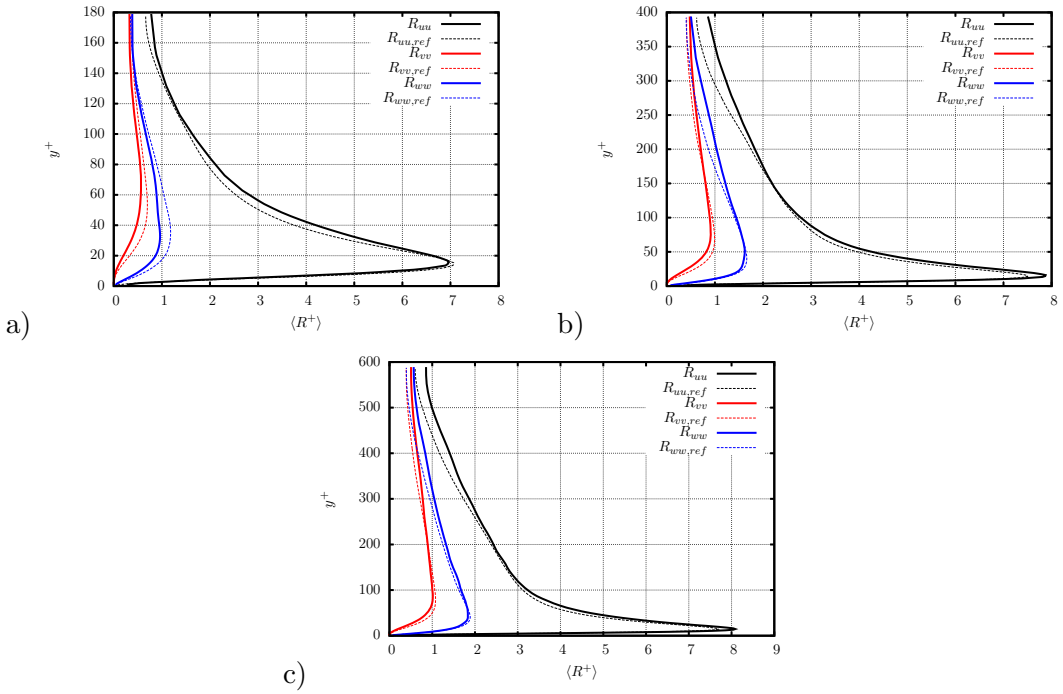

Figure 1: Cyclic channel flows: Reynolds stresses, a) $Re_\tau = 180$, b) $Re_\tau = 395$, c) $Re_\tau = 590$

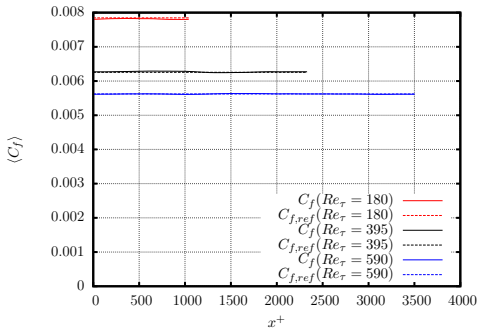

Figure 2: Cyclic channel flows: friction coefficients

create additional parasitic pressure noise. Thus in summary, aligning the structures by omitting R_{uv} produces better results.

In figure 4, the friction coefficient for all three considered Re_τ is shown, normalized by its respective asymptotic value. This shall illustrate the sensitivity of the synthetic turbulence to the Reynolds number. The figure indicates that the behavior is quite comparable, if the Reynolds number is sufficiently large. Then the adaption length has the same length in terms of dimensionless wall units. But if the Reynolds number is sufficiently low, the artificial turbulence does not survive. This is at least the case for the near-transition case of $Re_\tau = 180$.

A big advantage of the divergence-free vorton structures over continuity-breaching structures

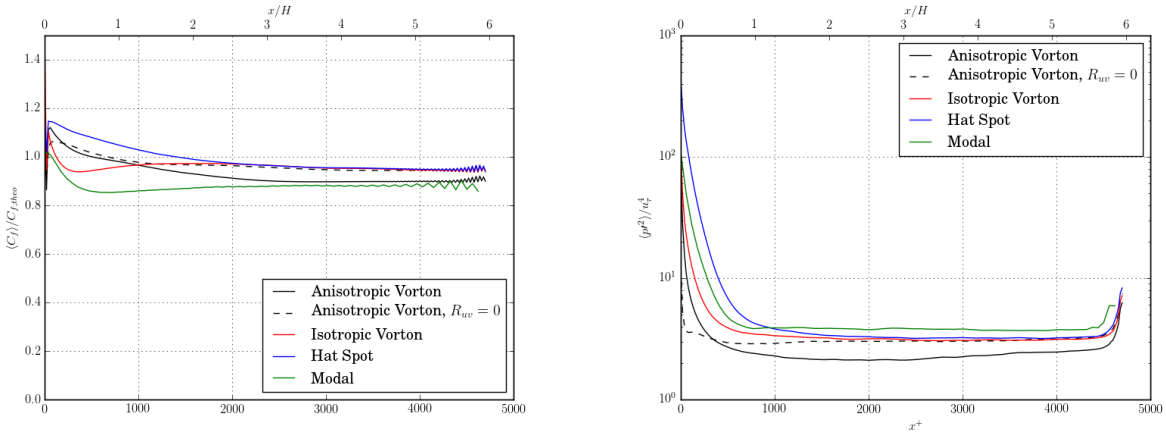

a) b)

Figure 3: Inflow channel simulations at $Re_\tau = 395$: comparison of a) friction coefficient b) pressure fluctuations vs. axial distance for different types of turbulent structures

like hat spots again becomes obvious from figure 3b: the artificial pressure noise is greatly reduced. While in the case of hat spots continuity is never fulfilled, isotropic vortons fulfill it only in the case of isotropy of the Reynolds stresses. Anisotropic vortons always fulfill continuity in the analytical case [1]. This is reflected by the hierarchy of curves in figure 3b. The largest artificial pressure noise is found for hat spots. That for anisotropic vortons is minimum while isotropic vortons are found in between. The difference between hat spots and anisotropic vortons is more than one order of magnitude.

5 SUMMARY

A novel type of turbulent spot has been derived. It allows fulfillment of the continuity constraint not only for isotropic Reynolds stresses but also for arbitrarily anisotropic ones.

The behavior of this structure has been demonstrated on a channel flow test case. Both case studies confirm that 1) the adaption length is positively influenced by application of vortons instead of simplicity-motivated velocity distributions like hat spots and 2) by being able to obey continuity always, the artificial pressure noise is greatly reduced.

6 LITERATURE

References

[1] Spille A. and Kaltenbach H. J. " Generation of turbulent inflow data with a prescribed shear-stress profile". In: *Third AFSOR Conference on DNS and LES* (2001), pp. 1–4.

[2] Dmitry Adamjan. "Method of synthetic turbulence generation on the inlet boundaries for the simulations of turbulent flows in vortex resolving approaches". (in russian). PhD thesis. St. Petersburg State Polytechnical University, 2011.

[1] When the velocity distribution of an anisotropic vorton is imposed on a discrete mesh, residual continuity errors arise again

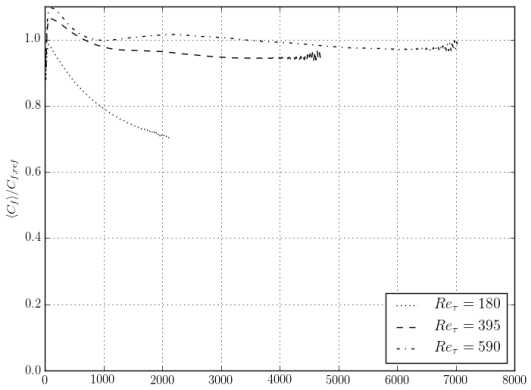

Figure 4: Inflow channel simulations: comparison of friction coefficient vs. axial distance for different Reynolds numbers (using the anisotropic vorton)

[3] N Jarrin et al. "A synthetic-eddy-method for generating inflow conditions for large-eddy simulations". In: *International Journal of Heat and Fluid Flow* 27 (2006), pp. 585–593.

[4] Hrvoje Jasak, Aleksandar Jemcov, and Zeljko Tukovic. "OpenFOAM: A C++ Library for Complex Physics Simulations". In: *International Workshop on Coupled Methods in Numerical Dynamics*. 2007.

[5] A Keating et al. "A priori and a posteriori tests of inflow conditions for large-eddy simulation ". In: *Physics of Fluids* 16.12 (2004), pp. 4696–4712.

[6] M Klein, A Sadiki, and J Janicka. "A digital filter based generation of inflow data for spatially developing direct numerical or large eddy simulations". In: *Journal of Computational Physics* 186.2 (2003), pp. 652–665.

[7] Nikolai Kornev and Egon Hassel. "A new method for generation of artificial turbulent inflow data with prescribed statistic properties for LES and DNS simulations". In: *Schiffbauforschung* 42.4 (2003), pp. 35–44.

[8] Nikolai Kornev and Egon Hassel. "Method of random spots for generation of synthetic inhomogeneous turbulent fields with prescribed autocorrelation functions". In: *Communications in Numerical Methods in Engineering* 23.1 (2007), pp. 35–43.

[9] Nikolai Kornev and Egon Hassel. "Synthesis of homogeneous anisotropic divergence-free turbulent fields with prescribed second-order statistics by vortex dipoles". In: *Physics of Fluids* 19.5 (2007).

[10] Thomas Lund, Xiaohua Wu, and Kyle Squires. "Generation of Turbulent Inflow Data for Spatially-Developing Boundary Layer Simulations". In: *Journal of Computational Physics* 140 (1998), pp. 233–258.

[11] Robert D Moser, John Kim, and Nagi N Mansour. "Direct numerical simulation of turbulent channel flow up to Re_τ= 590". In: *Physics of Fluids* 11.4 (1999), pp. 943–945.

[12] M. Pamies et al. " Generation of synthetic turbulent inflow data for large eddy simulation of spatially evolving wall- bounded flows". In: *Physics of Fluids* 21 (2009), p. 045103.

[13] C. D. Pierce and P. Moin. “Method for Generating Equilibrium Swirling Inflow Conditions”. In: *AIAA J.* 36 (1998), pp. 1325–1327.

[14] R. Poletto, T. Craft, and Revell A. “A New Divergence Free Synthetic Eddy Method for the Reproduction of Inlet Flow Conditions for LES”. In: *Flow, Turbulence and Combustion* (2013), pp. 519–539.

[15] J. U. Schlüter, H. Pitsch, and P. Moin. “ Large Eddy Simulation Inflow Conditions for Coupling with Reynolds-Averaged Flow Solvers”. In: *AIAA Journal* 42.3 (2004), pp. 478–484.

[16] S. Schmidt and M. Breuer. “ Extended Synthetic Turbulence Inflow Generator within a Hybrid LES-URANS Methodology for the Prediction of Non-Equilibrium Wall-Bounded Flows”. In: *Flow, Turbulence and Combustion* 95 (2015), p. 669.

[17] P. Spalart. “Direct simulation of a turbulent boundary layer up to $Re_\theta = 1410$ ”. In: *J. Fluid Mech.* 187 (1988), pp. 61–98.

[18] G. Tabor and M. Baba-Ahmedi. “ Inlet conditions for large eddy simulation: A review”. In: *Computers and Fluids* 39 (2010), pp. 553–567.

[19] Henry G. Weller et al. “A Tensorial Approach to Computational Continuum Mechanics Using Object-oriented Techniques”. In: *Comput. Phys.* 12.6 (Nov. 1998), pp. 620–631. ISSN: 0894-1866. DOI: 10.1063/1.168744. URL: http://dx.doi.org/10.1063/1.168744.